



# OPEN Effect of ultrasound-microbubble exposure on acute myeloid leukemia cancer cell proteome

Joelle Stilwell<sup>1,2,3</sup>, Daron A. Savaya<sup>1,2,3,4</sup>, Emmanuel Sakarya<sup>1,2,3</sup>, Charlotte Ferworn<sup>1,2,3</sup>, Eleanor Cloves<sup>4,5</sup>, Roberto J. Botelho<sup>4,5</sup>, Costin N. Antonescu<sup>4,5</sup> & Raffi Karshafian<sup>1,2,3</sup>✉

The application of ultrasound in combination with microbubbles (USMB) induces a broad spectrum of bioeffects on cells including plasma membrane disruption, cytoskeleton rearrangement, influx/efflux of cytosolic/extracellular molecules, metabolic stress and signalling pathways. This study investigated the effect of USMB on cell proteomics in human acute myeloid leukemia cells. Cells (OCI-AML-5) in suspension were exposed to ultrasound ( $f = 1$  MHz,  $PD = 20$   $\mu$ s and  $PRP = 1$  ms for 120 s) with and without microbubbles (Definity at 1.7% v/v) at varying acoustic pressures. Following exposure, cells were analysed using flow cytometry, mass spectrometry and immunoblotting. USMB enhanced cell membrane permeability (~37%), as expected, and induced significant changes in the cell proteome. Of 6825 proteins, 78 (~1.14%) were statistically significant and had a fold-change ( $\leq 0.8$  or  $\geq 1.2$ ) compared to untreated control, referred to as a differentially expressed protein (DEP). The highest fold change of ~4–5 was induced in HMOX1 protein. The protein expression depended on acoustic pressure, presence of microbubbles and elapsed-time following exposure to ultrasound. Western blotting analysis confirmed the effect of USMB on three proteins (HMOX1, BACH1 and ANXA1) with  $R^2$  values  $> 0.9$ . In addition, the gene ontology analysis based on DAVID bioinformatics indicated that the DEPs are associated with GO cellular components such as plasma membrane and exosomes, which can be affected by USMB. This study suggests that targeted changes in the cell proteome may be induced with USMB to potentially optimize existing therapies and develop new cancer therapeutic targets.

**Keywords** Ultrasound therapy, Microbubble, Sonoporation, Proteome, Acute myeloid leukemia

Expression of different proteins sets are responsible for enacting and regulating distinct cellular processes; consequently, manipulation of protein function is important in fields such as chemotherapy, where the protein expression is central to treatment effectiveness in diseases such as cancer, in particular for targeted therapies<sup>1</sup>. External factors such as chemical, thermal<sup>2</sup>, and mechanical stressors<sup>3</sup> can affect cellular function and gene and/or protein expression<sup>4,5</sup>. Therapeutic ultrasound in combination with microbubbles (USMB), a gas-filled and shell-encapsulated bubbles less than 5  $\mu$ m in diameter, can induce mechanical (cavitation), thermal, and chemical stresses on cells<sup>6</sup> and cause diverse bioeffects in cells and tissues<sup>7–11</sup>. The application of USMB is being developed as a targeted drug delivery strategy of various agents including chemotherapeutic<sup>12</sup> genetic<sup>13</sup> and nanoparticles<sup>14</sup>, and improve their efficiency through local release and enhanced intracellular uptake<sup>8,11,12,14</sup>. USMB has also been shown to enhance radiotherapy<sup>15</sup> and immunomodulation<sup>12</sup>. This study investigates, for the first time to the best of our knowledge, the effect of USMB on the cell proteome.

USMB mediated stressors can induce multiple bioeffect such as sonoporation which includes plasma membrane deformation and disruption<sup>8,9,16</sup> and increased rate of endocytosis by multiple distinct mechanisms<sup>11</sup>. In addition, USMB causes a stimulation of reactive oxygen species<sup>8</sup>, as well as activation of cell signalling and survival pathways<sup>17</sup>. The plasma membrane disruption induced by USMB can be irreversible leading to cell death, or transient/reversible cell membrane permeabilization, allowing for diffusion of molecules across the cell-membrane down their concentration gradient resulting in the uptake and leakage of molecules<sup>9–11,18,19</sup>. Consequently, the intracellular concentration of signaling molecules, such as calcium, can increase upon USMB

<sup>1</sup>Department of Physics, Toronto Metropolitan University, 350 Victoria Street, Toronto, ON M5B 2K3, Canada.

<sup>2</sup>Institute for Biomedical Engineering, Science and Technology (iBEST), A Partnership between Toronto Metropolitan University and St. Michael's Hospital, Toronto, ON, Canada. <sup>3</sup>Keenan Research Centre for Biomedical Science of St. Michael's Hospital, Toronto, ON, Canada. <sup>4</sup>Department of Chemistry and Biology, Toronto Metropolitan University, Toronto, ON, Canada. <sup>5</sup>Graduate Program in Molecular Science, Toronto Metropolitan University, Toronto, ON, Canada. ✉email: karshafian@torontomu.ca

treatment<sup>8</sup> whereas the intracellular metabolite levels, such as amino acids, and glycolytic and citric acid cycle intermediates, can decrease<sup>17</sup>. The USMB-induced plasma membrane deformation can also result in cytoskeletal rearrangement<sup>8</sup>, as the actin cytoskeleton is centrally involved in generating and responding to mechanical forces<sup>20</sup>. It has been shown that the number of f-actin fibres increases due to USMB<sup>21</sup>. In addition, USMB can increase in the rate of endocytosis of both clathrin-mediated endocytosis and non-clathrin fluid-phase uptake into cells<sup>11,22,23</sup> as well as exocytosis<sup>9</sup>. In addition, USMB can modulate diverse signaling networks involved in regulating cell survival, metabolism<sup>17</sup> apoptosis<sup>24</sup> and cell cycle<sup>25</sup>.

The cell surface plays a large role in sensing stress as its components transmit extracellular stimuli to the intracellular environment<sup>26</sup>. The initial response of the cell to a stressful stimulus is aimed toward cell survival and defending or recovering from cellular damage. In signal transduction, extracellular stimuli are relayed through intracellular proteins initiating a cellular response<sup>27</sup>. Changes in protein expression can result from changes in protein synthesis, through regulation of transcription and/or translation of specific genes, or alternatively, regulation of protein turnover. USMB treatment can lead to alterations of the rate of protein internalization from the cell surface, a phenomenon that can in principle regulate the composition of proteins at the cell surface<sup>11</sup>, either by leading to relocation of proteins from the plasma membrane into intracellular membrane compartments, or traffic of cell surface proteins to the lysosome for degradation.

The guiding hypothesis of this study is that USMB-induced stress affects the cell proteome in response to the broad spectrum of cellular and molecular associated bioeffects. We investigated the bioeffects of USMB on AML cells; specifically, sonoporation and proteomics using flow cytometry, mass spectrometry (MS) and western blot (WB) over 24 h. Improving our understanding of USMB induced cellular responses on the proteomic level may provide insights for developing novel USMB based therapeutic strategies.

## Materials and methods

### In vitro model

Human Acute Myeloid Leukemia AML (OCI-AML-5) (henceforth AML cells) were used as the in vitro model. The AML cells were cultured in AMEM (Alpha Modification of Eagles Medium, Wisent Biocenter, Cat. No. 310-010-CL) supplemented with 10% FBS (Fetal Bovine Serum, Sigma-Aldrich, Cat. No. F1051) and 1% P/S (Penicillin/Streptomycin, Wisent Biocenter, Cat. No. 450-201-EL) in a humidified incubator at 37 °C and 5% CO<sub>2</sub>.

### USMB exposure

An overview of the experimental study is shown in Fig. 1. Cells at a concentration of  $1.33 \times 10^6$  cells/mL (7 million cells in 3 mL of AMEM, Wisent Biocenter, Cat. No. 310-010-CL) were treated in suspension with a tone-burst pulse at 1 MHz center frequency transducer (A394S-SU-F2.00IN-PTF, Olympus, Waltham, MA, USA) with diameter = 28.6 mm, -6 dB focal length = 54 mm, and -6 dB beamwidth = 3.8 mm. The US exposure has a pulse repetition period (PRP) = 1 ms; pulse duration period (PDP) = 20  $\mu$ s corresponding to duty cycle of 2%; and insonation time (IT) = 120 s<sup>28</sup>. The cells were treated at 1.7% (v/v) Definity (Lantheus Medical Imaging, Billerica, MA, USA) microbubble concentration (100  $\mu$ L of diluted MB at 1:1 ratio with PBS) and varying peak negative pressures (0–950 kPa). Before treatment, the Definity vials were left at room temperature for 30 min before being activated in a Vial Mix (Lantheus Medical Imaging, Billerica, MA, USA) for 45 s. The vial was then equilibrated before being inverted and vented with a needle. After venting, the microbubbles were extracted at 1.7% (v/v) and diluted with an equal amount of PBS<sup>28</sup>.

### Flow cytometry

#### Cell permeability and viability

Cell permeability was explored by treating the cells with USMB with the addition of 10 kDa FITC-Dextran (Cat. No. FDS10S, Sigma Aldrich). A volume of 70  $\mu$ L of 5 mg/mL FITC-Dextran was added to a sample of cells immediately before treatment. After treatment, cells were incubated at 37 °C for 30 min. Cells were then washed three times with PBS (Wisent Biocenter, Cat. No. 311-010-CL) before being resuspended in 1 mL FACS buffer (PBS and 2% FBS) with PI (Cat. No. P3566, ThermoFisher Scientific) at a concentration of 0.0001 mg/mL immediately before analysis with the SONY SP6800 flow cytometer (Sony Biotechnology, San Jose, CA, U.S.A.).

#### Flow cytometry analysis

Flow Cytometry data was analyzed using FlowJo™ v10.8 Software (BD Life Sciences). The sample was gated based on FSC-A and SSC-A, and FSC-A and FSC-H to identify intact single cells within the population of all events recorded on the cytometer. Following this, live cells (PI negative) and permeabilized cells (FITC positive and PI negative) were quantified.

#### Proteomics sample preparation

Mass Spectrometry and Western Blot samples were prepared simultaneously for direct comparisons. Following the treatment, cells were counted and split into  $9 \times 10^6$  cells for Mass Spectrometry and  $5 \times 10^6$  cells for Western blots. For mass spectrometry analysis, cells were treated at the following conditions: USMB at 450 kPa (6 h) and 750 kPa (6 and 24 h), and US only at 750 kPa (6 h). For Western Blot analysis, cells were treated with USMB at three pressures (350, 450 and 750 kPa) and US only at 750 kPa at three different time points (1, 6 and 24 h).

### Mass spectrometry

#### Sample preparation

Following incubation and cell counting, the cells were collected by centrifugation at 300 g for 5 min, and the supernatant was discarded. Cells were washed twice in PBS and centrifuged for 300 g for 5 min. The mass of the

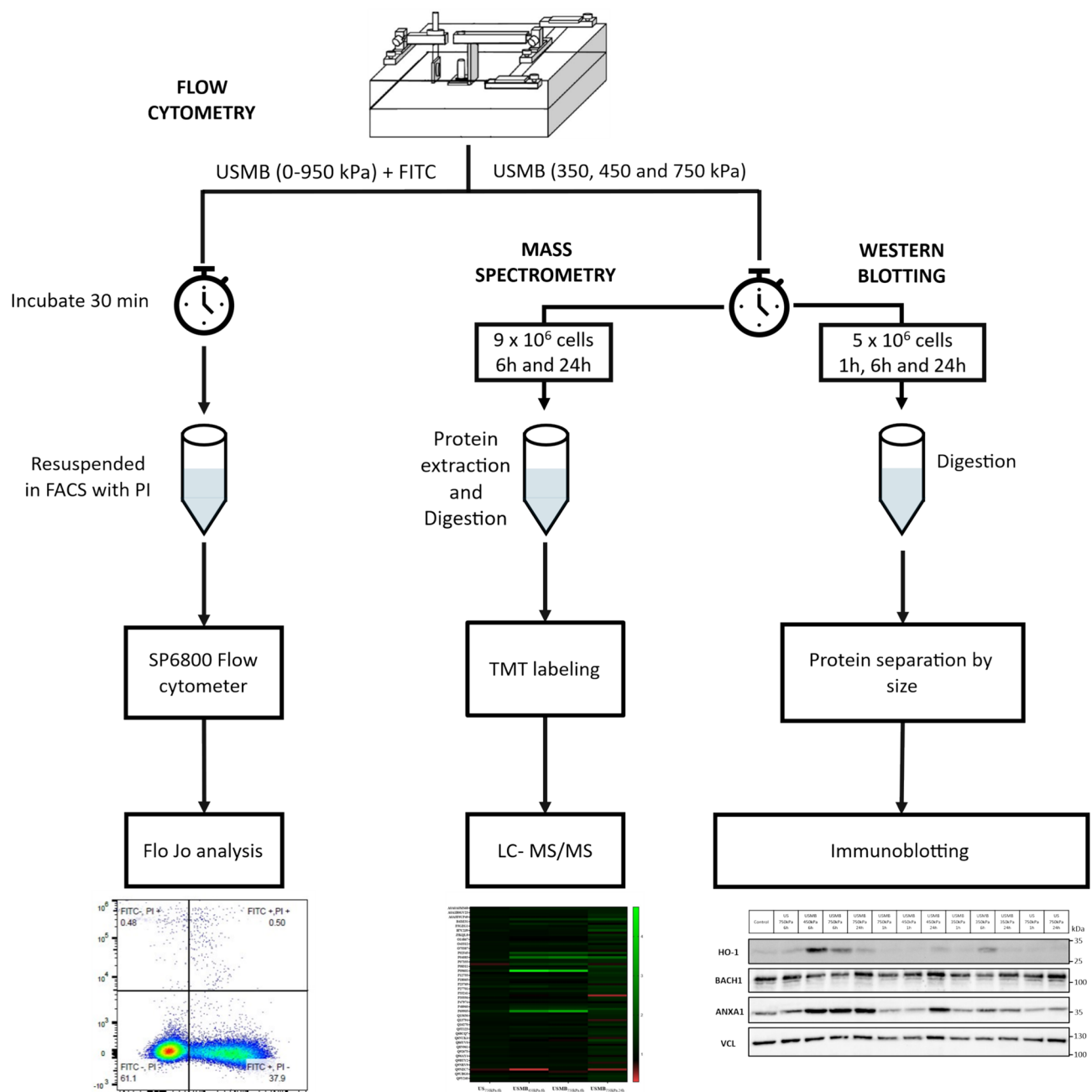


**Fig. 1.** Schematic diagram of the experimental design and analysis. Flow cytometry (left branch) was used to measure the uptake of FITC and PI at US (950 kPa) and USMB (0-950 kPa). Following USMB with FITC, the sample was incubated (37 °C) for 30 min. PI was added prior to analysis of cells with flow cytometry. Cells prepared and treated simultaneously and split for MS and WB analysis (center and right branch). MS and WB cells went through their respective digestions and preparation for analysis. TMT labelling was done for analysis through MS. WB lysates were prepared for immunoblotting.

wet pellet was measured, and RIPA Lysis and Extraction buffer (Cat. No 89900, ThermoFisher) was combined with protease inhibitors (Cat No.11836170001, Sigma-Aldrich (St. Louis, Mo)). The RIPA and protease mixture was added according to weight (1 mL/40 mg of wet cell pellet). The cells were resuspended and subsequently frozen for preparation by SPARC Biocentre. Protein reduction, alkylation, precipitation, digestion, fractionation, TMT labelling and LC- MS/MS (liquid chromatography – mass spectrometry) were performed by SPARC Biocentre (Molecular Analysis), The Hospital for Sick Children, Toronto, Canada. All samples were sonicated at 4 W for 15 s before being clarified by centrifugation at 10,000 g for 5 min. 150 µL of each sample was taken for protein digestion. To reduce the sample, 10 mM of TCEP was added at 60 °C for 1 h. Following reduction, alkylation was performed with 18.75 mM of iodoacetamide at room temperature for 30 min in the dark. Protein

precipitation was carried out using acetone at  $-20^{\circ}\text{C}$  for 2.5 h. The proteins were then digested with 3  $\mu\text{g}$  Trypsin/Lys-C per sample, at  $37^{\circ}\text{C}$  overnight in 100 mM TEAB. For peptide quantification the Peirce Colorimetric Peptide Quant kit was used and 50  $\mu\text{g}$  of protein were labelled per sample. Tandem mass tag (TMT) labelling was performed with 50  $\mu\text{g}$  from each sample. The 50  $\mu\text{g}$  samples of peptides were dissolved in 100 mM HEPES (pH 8.5) and labelled with 0.5 mg TMT Pro reagent at room temperature for 1 h, while shaking. Excess TMT Pro reagent was quenched with 5  $\mu\text{L}$  5% hydroxylamine for 15 min while shaking. After quenching, samples were combined and dried in SpeedVac. Dried proteins were fractionated using a high pH fractionation gradient; 60 fractions were collected and dried in SpeedVac. Samples were then resuspended in 2% ACN, 0.1% formic acid, and loaded onto EvoSep Evotips.

### Analysis

Proteome discoverer version 2.5.0.400 was used as a protein identification and quantification software. Data generation was performed by SPARC Biocentre (Molecular Analysis), The Hospital for Sick Children, Toronto, Canada. The proteins were then sorted by their False Discovery Rate (FDR) confidence. The software assigned each protein a value of low, medium, or high confidence in their discovery. Subsequently, proteins with 2 or more unique peptides having high FDR confidence were considered for statistical analysis; these proteins are referred to as detected proteins.

## Immunoblotting

### Sample preparation

Following incubation and cell counting, cells were collected by centrifugation at 300 g for 5 min, and the supernatant was discarded. Cells were washed twice in PBS and centrifuged for 300 g for 5 min. The mass of the wet pellet was measured, and RIPA Lysis and Extraction buffer (Cat. No 89900, ThermoFisher Scientific, MA, USA) was combined with protease inhibitors (Cat No.11836170001, Sigma-Aldrich (St. Louis, Mo) and phosphate inhibitors (Cat. No 4906845001, Sigma-Aldrich (St. Louis, Mo)). This mixture was added according to weight (1 mL/40 mg of wet cell pellet). RIPA buffer was added to the pellet and shaken on ice for 15 min. The mixture was centrifuged at 14,000 g for 15 min, and the pellet was discarded. The supernatant was transferred to a different tube and frozen.

### SDS-PAGE and immunoblotting

The protein concentration of lysates was determined using the Pierce BCA protein assay. A 15  $\mu\text{g}$  of protein lysate was mixed with Laemmli Sample Buffer and 2-mercaptoethanol. Proteins were denatured by exposing samples to  $100^{\circ}\text{C}$  for 10 min on a heat block. Samples were loaded on a 12% polyacrylamide gel, separated by mass via gel electrophoresis, and transferred onto a polyvinylidene fluoride (PVDF) membrane. PVDF membranes were incubated with blocking solution (5% skim milk, BioRad) in tris-buffered saline and tween-20 (TBS-T; 20 mM Tris, 150 mM NaCl, 0.1% Tween-20) for 1 h at room temperature. Membranes were incubated with a primary antibody overnight at  $4^{\circ}\text{C}$ , washed with TBS-T ( $4 \times 5$  min), incubated with a secondary antibody conjugated to horseradish peroxidase (1 h at room temperature), and washed with TBS-T ( $4 \times 5$  min). Membranes were soaked with Immobilon Crescendo Western HRP substrate (Millipore Sigma; cat: WBLUR0500) for 1 min and HRP was detected using a gel doc instrument. The primary antibodies used were rabbit anti-HMOX1 (1:1000 in blocking solution; Proteintech; cat: 10,701-1-AP), rabbit anti-BACH1 (1:1000 in blocking solution; Proteintech; cat: 14,018-1-AP), rabbit anti-Annexin-A1 (1:1000 in blocking solution; Proteintech; cat: 21,990-1-AP), and mouse anti-Vinculin (1:1000 in blocking solution). Secondary antibodies used were goat anti-rabbit (1:1000 in blocking solution; Cell Signaling Technology; cat: 7074) and goat anti-mouse (1:1000 in blocking solution; Cell Signaling Technology; cat: 7076). Membranes were stripped with Stripping Buffer for 10 min at room temperature. Subsequently, BACH1 and HO-1 were probed simultaneously, followed by VCL and ANXA1 the next day.

Analysis: Images were acquired using a chemiluminescent substrate. Quantification was conducted using FIJI software<sup>29</sup>. The bands were analyzed individually via the ImageJ ROI feature, which generated an intensity profile for each band. Relative to the background, the area under each peak was identified, corresponding to the integrated pixel density of each band. Finally, the integrated pixel density of the protein of interest was normalized to the VCL loading control from the same lane to account for loading variation. These normalized values were used in further analyses.

## Statistical analysis

The detected proteins (2 or more unique peptides and high FDR confidence) were tested for statistical significance using GraphPad PRISM (Version 10.3.1). Identified proteins refer to the detected proteins which were statistically significant (unadjusted  $p$ -value  $\leq 0.05$ ) compared to the untreated control. A differentially expressed proteins (DEP) is classified as any identified protein ( $p \leq 0.05$ ) with a MS-detected fold-change ( $\text{FC}_{\text{MS}}$ ) value  $\geq 1.2$  or  $\leq 0.8$ , relative to the untreated control condition. These criteria are used to identify upregulated and downregulated protein expressions, respectively. A non-DEP is classified as any identified protein ( $p \leq 0.05$ ) with a  $\text{FC}_{\text{MS}}$  value between 0.8 and 1.2, non-inclusive. A two-way ANOVA test was conducted to test the interaction between proteins and treatments, with a post-hoc Tukey's multiple comparisons test of all samples.  $P$ -values of  $\leq 0.05$  are considered significant.

## Results

### Sonoporation

Cell permeability and viability following exposure to ultrasound in the absence (Pneg: 950 kPa) and presence of microbubbles (Pneg: 0-to-950 kPa) are shown in Figs. 2A,B, respectively. Ultrasound alone at the exposure

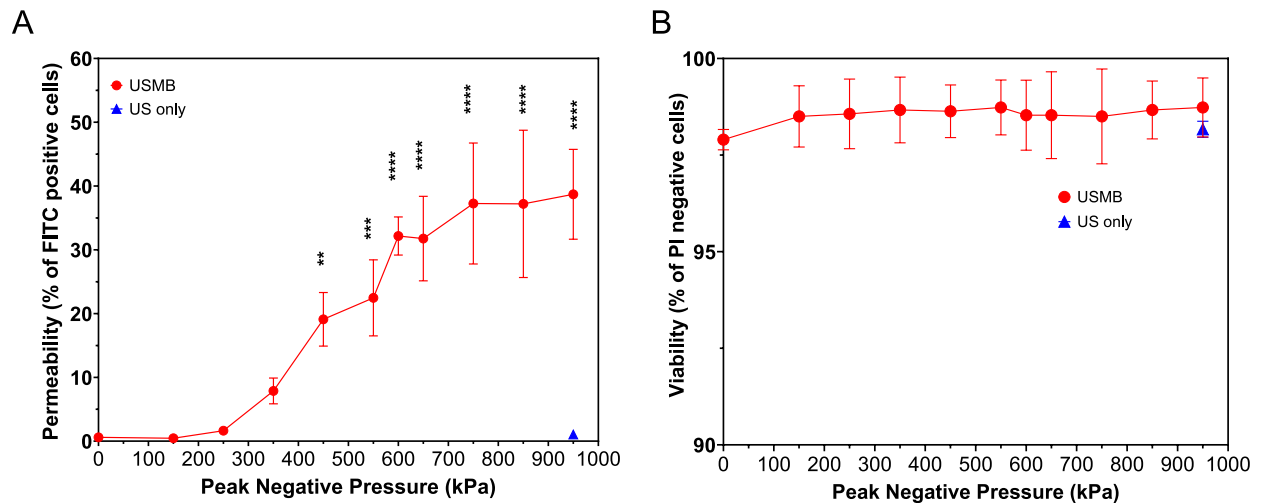


**Fig. 2.** (A) Cell permeability, the percentage of FITC-dextran (10 kDa) positive cells, and (B) cell viability, the percentage of PI negative cells, 30 min following exposure to US only (triangle) at 950 kPa and USMB (circle) at 0–950 kPa peak negative pressures. Permeability was induced in the presence of microbubbles and increased with pressure reaching a plateau. Cell viability remained consistent across all conditions. The mean and SD of the FITC positive and PI negative populations are shown for  $n=3$  independent experiments. The p-value threshold represented by \*  $p \leq 0.05$ , \*\*  $p \leq 0.01$ , \*\*\*  $p \leq 0.001$ , and \*\*\*\*  $p \leq 0.0001$ .

conditions of this study did not significantly increase the percentage of permeabilized cells or decrease cell viability, as expected<sup>10,28</sup>. In contrast, following treatment with USMB, cell permeability increased with acoustic pressure up to a plateau of ~38%, and with statistical significance at pressures greater than and equal to 450 kPa compared to untreated control (Fig. 2A). In addition, cell viability (~99%) was similar across all exposure conditions; no statistical difference was observed (Fig. 2B). The sonoporation bioeffect appears to start at 250–350 kPa with an average of 8% FITC positive population at 350 kPa, although not statistically significant compared to untreated control (~0.6%). The number of permeabilized cells appears to increase with acoustic pressure and reach a plateau around 750–850 kPa. Cell permeability approximately doubled between 350 kPa (~8%) and 450 kPa (~19%), and subsequently doubled between 450 kPa (~19%) and 750 kPa (~37%). Based on the cell permeability data, the ultrasound pressures used in the investigation of the effect of USMB on the cell proteome are 350, 450 and 750 kPa peak negative pressure.

### Cell proteome

Cells were exposed to USMB at different exposure conditions and analysed for proteome changes. The samples comprised of entirely viable cells (~99%) included both sonoporated (FITC positive) and non-sonoporated (FITC negative) cells. The percentage of sonoporated cells depended on the ultrasound pressure; 8%, 19% and 37% for 350, 450 and 750 kPa, respectively (Fig. 2A). Based on the MS analysis, a total of 6825 proteins were detected. Of the 6825 detected proteins, a total of 1683 proteins (~25%) in at least one of the four treatment conditions (US<sub>750kPa,6 h</sub>, USMB<sub>450kPa,6 h</sub>, USMB<sub>750kPa,6 h</sub> and USMB<sub>750kPa,24 h</sub>) were statistically significant (post-hoc Tukey test) compared to the untreated control, referred to as statistically identified proteins. Furthermore, of the statistically identified proteins, 78 proteins (~5% of 1683) had a  $FC_{MS}$  (fold-change in protein expression compared to untreated control based on MS)  $\leq 0.8$  or  $\geq 1.2$ . These 78 proteins (1.1% of 6825) are referred to as differentially expressed proteins (DEPs); that is, a protein that has a high confidence in its discovery with  $\geq 2$  unique peptides with a  $FC_{MS} \leq 0.8$  or  $\geq 1.2$  and a p-value  $\leq 0.05$  compared to the untreated control.

The MS data for each of the four treatment conditions (US<sub>750kPa,6 h</sub>, USMB<sub>450kPa,6 h</sub>, USMB<sub>750kPa,6 h</sub> and USMB<sub>750kPa,24 h</sub>) are shown as volcano plots in Fig. 3A–D, respectively. The corresponding heatmap of the 78 DEPs, referred to as DEP<sub>78</sub>, demonstrates the expression changes throughout all the conditions and is shown in Fig. 3E (further information in Table S1). The Venn diagram of the 77 DEPs from the three USMB conditions (US alone condition excluded), referred to as DEP<sub>77</sub>, including both up- or down-regulated proteins, are shown in Figs. 3F–H, respectively. The changes in the cell proteome depended on the ultrasound exposure conditions and the elapsed-time following ultrasound. The presence of microbubbles was necessary to induce changes in the cell proteome (Figs. 3A,C). The number of DEPs and the overall  $FC_{MS}$  increased significantly in the presence of microbubbles compared to ultrasound alone (Table S1). At US<sub>750kPa,6 h</sub>, only one DEP was identified compared to 12 DEPs at USMB<sub>750kPa,6 h</sub>. The effect of the acoustic pressure appears to be less pronounced compared to the effect of microbubbles; 17 DEPs (US<sub>450kPa,6 h</sub>) compared to 12 DEPs (USMB<sub>750kPa,6 h</sub>) when acoustic pressure increases from 450 to 750 kPa with a similar average  $FC_{MS}$  value of 1.15 (Fig. 3B,C). There is an overlap of 11 DEPs between the two pressures (450 and 750 kPa) where all are up regulated (Fig. 3F–H). These results indicate that the presence of microbubbles was critical to elicit DEP, and that acoustic pressure impacted a subset of the DEPs triggered by USMB.



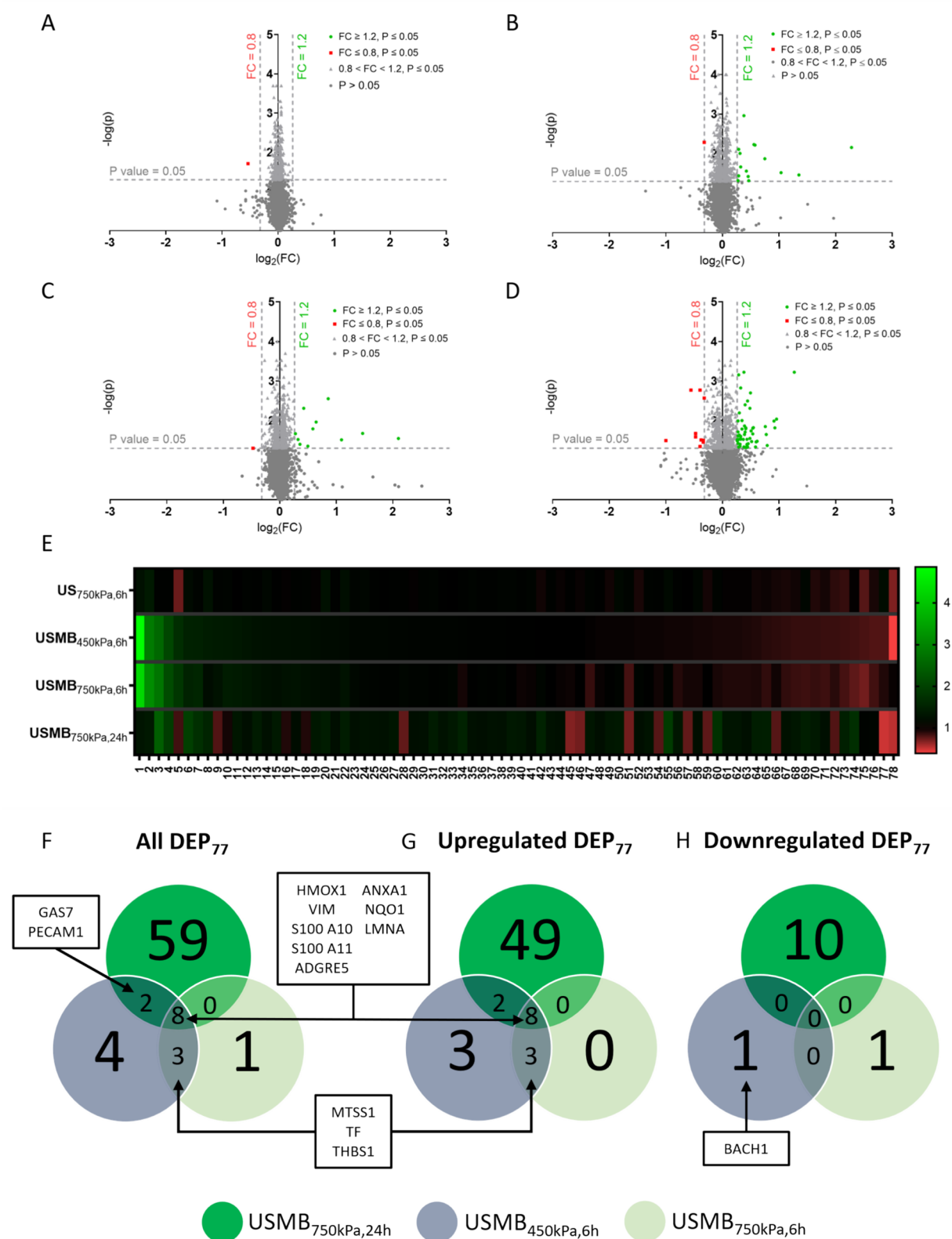


**Fig. 3.** Volcano plots of proteins in (A) US<sub>750kPa,6h</sub>, (B) USMB<sub>450kPa,6h</sub>, (C) USMB<sub>750kPa,6h</sub>, and (D) USMB<sub>750kPa,24h</sub>. DEPs are represented by green (upregulated) and red (downregulated) points; by definition, DEPs are statistically significant with a threshold of  $p \leq 0.05$ . A list of the p-values for all DEPs (relative to untreated control) are included in Table S1, located in the supplementary file. E) Heat map showing the 78 DEPs (listed in Table S1).  $FC_{MS}$  is plotted on the y axis and shows  $FC_{MS}$  only (not statistical significance). Proteins may not be DE at each condition. Plotted values are the mean  $FC_{MS}$  for each protein with  $n = 3$  independent experiments. Comparison of the number of DEPs at USMB<sub>450kPa,6h</sub>, USMB<sub>750kPa,6h</sub> and USMB<sub>750kPa,24h</sub> for F) DEP<sub>77</sub>, G) DEP with  $FC_{MS} \geq 1.2$  and H) DEPs with  $FC_{MS} \leq 0.8$ .

There are several DEPs that are upregulated in response to various USMB treatments, including Annexin A1 (ANXA1), S100-A10 and A11, NADPH dehydrogenase quinone 1 (NQO1), prelamin A/C (LMNA), vimentin (VIM), heme oxygenase 1 (HMOX1), adhesion G coupled receptor E5 (ADGRE5), metastasis suppressor protein 1 (MTSS1), serotransferrin (TF) and thrombospondin-1 (THBS1) (Figs. 3F-H). There is no common downregulated DEP among any of the conditions. Transcription regulator protein BACH1 (BACH1) is the only downregulated DEP at 450 kPa pressure. The effect of time appears to be more pronounced on the number of DEPs; 12 DEPs at 6 h compared to 69 DEPs at 24 h following USMB treatment at 750 kPa. The USMB<sub>450kPa,6 h</sub> and USMB<sub>750kPa,24 h</sub> had overall FC<sub>MS</sub> (78 DEPs) of 1.15 and 1.24, respectively. However, the overlap in the DEPs between the two times (6 and 24 h) is comparable to the effect of the acoustic pressure (Figs. 3G-H). The first eight proteins stated above are common between the three USMB conditions. Furthermore, two DEPs are common between the 6 and 24 h timepoints. These are growth arrest-specific protein 7 (GAS7) and platelet endothelial cell adhesion molecule (PECAM1) (Figs. 3 G-H).

While there were many DEPs that were common to multiple different USMB treatment pressures and elapsed-time following USMB, there were also some DEPs that were unique to specific treatments. The largest number of unique DEPs that are either up- or downregulated is with USMB treatment at 750 kPa and 24 h following exposure; of the 78 proteins, 66 were upregulated and 12 were downregulated. Based on their expression in overall USMB exposure conditions, 14 proteins were selected for further analysis. Within this subset, 8 proteins were identified as DEPs across all 3 USMB conditions, and 5 proteins were common between at least two USMB conditions. BACH1 was added to this subset as the only downregulated protein at the USMB<sub>450kPa,6 h</sub> condition and for its role in the regulation of HMOX1. The list of these 14 DEPs (referred to as DEP<sub>14</sub>) and their fold-change are shown in Fig. 4 and Table 1.

#### DEP<sub>14</sub>: Mass spectrometry

The FC<sub>MS</sub> of the DEP<sub>14</sub> from the four treated conditions (US<sub>750kPa,6 h</sub>, USMB<sub>450kPa,6 h</sub>, USMB<sub>750kPa,6 h</sub> and USMB<sub>750kPa,24 h</sub>) are shown in Fig. 4, and the statistical comparison between the different conditions for each DEP (DEP<sub>14</sub>) is shown in Table S2. US alone did not induce any statistically significant effect on the 14 DEPs compared to the control. The largest FC<sub>MS</sub> was observed in heme oxygenase (HMOX1) protein; a comparable FC<sub>MS</sub> of ~4–5 was achieved with USMB at both 450 and 750 kPa within 6 h following exposure. The transcription regulator protein BACH1 (BACH1) of the DEP<sub>14</sub> was downregulated with FC<sub>MS</sub> ~0.8 at USMB<sub>450kPa,6 h</sub>, with statistical significance compared to control. When comparing the common DEPs at 450 and 750 kPa pressures, only one DEP has a significant difference in FC<sub>MS</sub>, this is prelamin A/C, with FC<sub>MS</sub> of 2.02 and 2.11 for USMB<sub>450kPa,6 h</sub> and USMB<sub>750kPa,6 h</sub>, respectively. Noteworthy, 8 of the 11 proteins (S100A10, A11, HMOX1, ANXA1, NQO1, LMNA, VIM, and ADGRE5) are differentially expressed in all USMB conditions, highlighting the dependence of microbubbles in triggering changes expression upon ultrasound exposure. NQO1 and LMNA, also display time and pressure dependence, respectively. Focusing on NQO1, USMB<sub>6h</sub> samples are significantly different

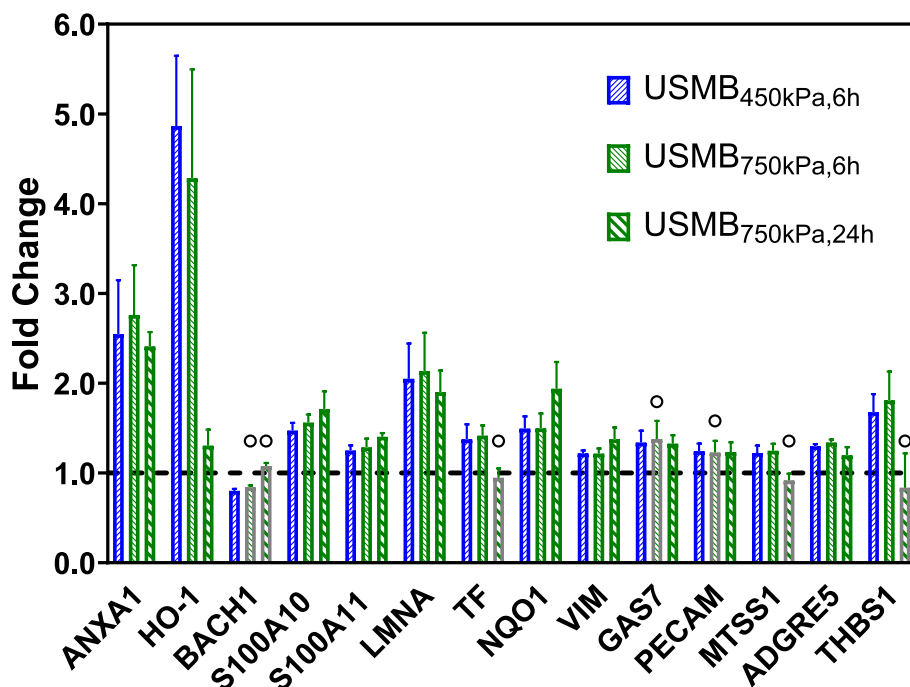


**Fig. 4.** FC<sub>MS</sub> for the 14 proteins listed in Table 1 for the three USMB treated conditions (USMB<sub>450kPa,6 h</sub>, USMB<sub>750kPa,6 h</sub> and USMB<sub>750kPa,24 h</sub>) are shown as mean ± SD for n = 3 independent experiments. Nonsignificant conditions relative to the untreated control are indicated with a circle (O) and have grey-colored borders (the statistical significance is stated in Table S1).

Protein Accession	Protein name (gene name)	USMB	USMB	USMB
		450 kPa,6 h	750 kPa,6 h	750 kPa,24 h
P09601	Heme oxygenase 1 (HMOX1)	4.86	4.28	1.3
B4DLR8	NAD(P)H dehydrogenase [quinone] 1 (NQO1)	1.49	1.5	1.94
P02545	Prelamin-A/C (LMNA)	2.05	2.13	1.9
P04083	Annexin A1 (ANXA1)	2.55	2.76	2.41
P08670	Vimentin (VIM)	1.22	1.21	1.37
P31949	Protein S100-A11 (S100A11)	1.25	1.28	1.4
P48960	Adhesion G protein-coupled receptor E5 (ADGRE5)	1.3	1.34	1.2
P60903	Protein S100-A10 (S100A10)	1.47	1.56	1.71
O43312	Protein MTSS 1 (MTSS1)	1.22	1.25	N/A
P02787	Serotransferrin (TF)	1.37	1.41	N/A
P07996	Thrombospondin-1 (THBS1)	1.68	1.81	N/A
A0A0A0MS68	Growth arrest-specific protein 7 (GAS7)	1.34	N/A	1.33
P16284	Platelet endothelial cell adhesion molecule (PECAM1)	1.24	N/A	1.23
O14867	Transcription regulator protein BACH1 (BACH1)	0.8	N/A	N/A

**Table 1.** Differentially Expressed Proteins of interest (DEP<sub>14</sub>), up-regulated ( $FC_{MS} \geq 1.2$  and  $p\text{-value} \leq 0.05$ ) and down-regulated DEPs ( $FC_{MS} \leq 0.8$  and  $p\text{-value} \leq 0.05$ ), across the three USMB treatment conditions. NA indicates the conditions that are not statistically significant ( $p > 0.05$ ).

compared to the USMB<sub>750kPa,24 h</sub> condition (Supplementary Table 2), confirming that time does influence the expression at 6 and 24 h. LMNA has significant differences between its USMB<sub>450kPa,6 h</sub> and USMB<sub>750kPa,6 h</sub> conditions, which denotes that pressure directly effects the expression in addition to the presence of MBs. Three proteins (HMOX1, BACH1 and ANXA1,) out of DEP<sub>14</sub>, referred to as DEP<sub>3</sub>, are used to confirm the MS observations, by Western blotting (WB). Additional ultrasound conditions (US at Pneg: 750 kPa and USMB at Pneg: 350, 450 and 750 kPa) and times (1, 6 and 24 h) following the treatment, were investigated with WB; a total of 12 conditions.

**WB of DEP3: WB of HMOX1, BACH1 and ANXA1**

The WB data of the DEP<sub>3</sub> (HMOX1, BACH1 and ANXA1) are shown Figs. 5A-B, and their corresponding MS data in Fig. 5C. In general, the WB data confirms the MS data for the three proteins (DEP<sub>3</sub>). WB analysis confirmed the MS observations. There is high correlation between  $FC_{MS}$  and  $FC_{WB}$  data for the DEP<sub>3</sub>;  $R^2$  values of 0.9771, 0.9003 and 0.9716 for HMOX1, BACH1 and ANXA1, respectively (Figure S1). HMOX1 expression increased with the presence of microbubbles, peaked at the 6 h time point and was maximum at 450 kPa (Fig. 5B). No statistical changes in  $FC_{WB}$  were observed in the absence of microbubbles at 750 kPa and all time points, whereas significant increase in  $FC_{WB}$  was observed with the addition of microbubbles at 750 kPa and the 6 h. No statistical  $FC_{WB}$  was observed at 1 and 24 h time points in HMOX1 at all ultrasound-treated conditions compared to untreated control. HMOX1's expression depended significantly on the time following ultrasound exposure. It remained steady within the first hour, increased significantly by the 6 h reaching a peak, and then decreased by 24 h down to control levels (Fig. 5B). This supports the changes in HMOX1 expression as observed by MS (Fig. 5E), indicating that the increase in HMOX1 expression is transient. The  $FC_{WB}$  of HMOX1, identified as a DEP through mass spectrometry at the USMB conditions 450 kPa (6 h) and 750 kPa (6 h and 24 h), was statistically significant compared to untreated control at USMB at 450 kPa and 750 kPa (6 h). The maximum  $FC_{WB}$  depended on the US pressure; the highest increase was observed at 450 kPa ( $FC_{WB} \sim 10$  and  $FC_{MS} \sim 5$ ) compared to 750 kPa ( $FC_{WB} \sim 7$  and  $FC_{MS} \sim 4$ ).

BACH1, was the only DEP with a  $FC_{MS}$  of  $\sim 0.8$  (Fig. 5F), although on average showed a lower  $FC_{WB}$  of  $\sim 0.74$ , it was not statistically different compared to untreated control (Fig. 5C). On average, BACH1 appears to decrease by 6 h following USMB at 450 kPa, and recover within 24 h. However, statistically there was no difference between the different exposure conditions and times. Furthermore, the BACH1 and HMOX1 appear to be inversely related (Fig. 5B,C). The ANXA1 WB confirmed the MS data (Figs. 5D,G). ANXA1 has been identified as a DEP through mass spectrometry at all USMB treated conditions (Fig. 5G). The ANXA1  $FC_{WB}$  increased with the addition of microbubbles ( $FC_{WB} \sim 2.8\text{--}3.1$ ). Generally, the  $FC_{WB}$  increased with time and almost reached a plateau at 6 h (Fig. 5D). Statistically significant  $FC_{WB}$  was observed at USMB 750 kPa at both 6 and 24 h. In addition, the ANXA1 expression increased with acoustic pressure, similarly to HMOX1. The ANXA1  $FC_{WB}$  at 450 kPa and 750 kPa were significantly different compared to 350 kPa. The WB analysis confirmed and expanded on the MS observations. Overall, the expression of HMOX1 and ANXA1 depends on the exposure conditions and time following USMB, insinuating that USMB-induced bioeffects on the cell proteome may be transient and associated with the biomechanical stress. The highest  $FC_{MS}$  was observed at 450–750 kPa and 6 h; the acoustic pressure appears to be consistent with the sonoporation analysis.

**Gene Ontology cellular components**

DAVID Bioinformatics<sup>30,31</sup> was used to generate a list of Gene Ontology (GO) cellular components with the statistically identified proteins (1683), DEP<sub>78</sub> and DEP14 (Fig. 6). DAVID, based on the protein list defined by



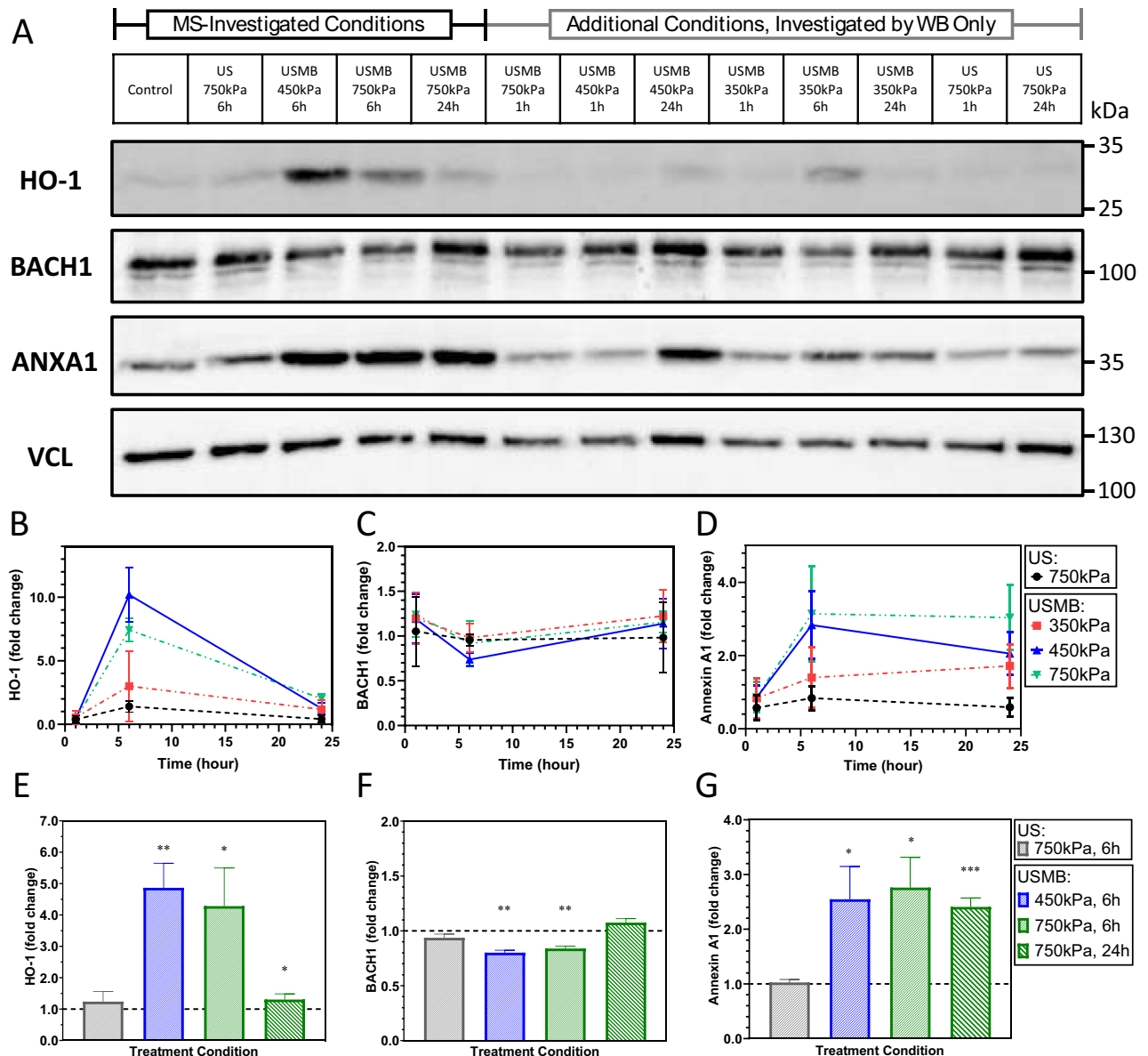
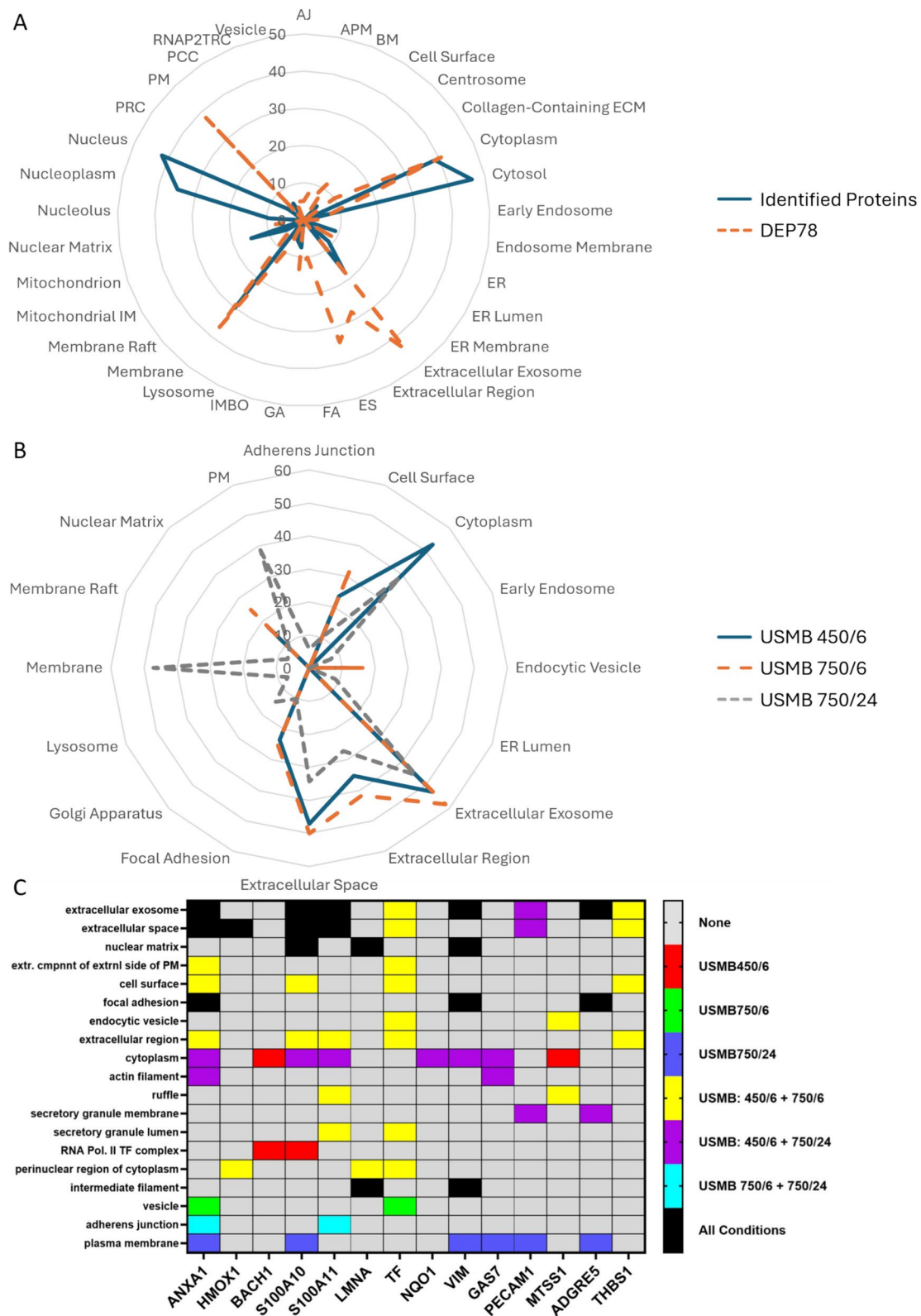


**Fig. 5.** A representative western blot and the fold changes for the DEP<sub>3</sub> (ANXA1, HMOX1 and BACH1): (A) Representative western blot analyzing the relative levels of the DEP<sub>3</sub> with the sample for each treatment condition shown vertically and the proteins in each row; Vinculin was used as the loading control. Whole gel images of WB snippets are presented in Figure S2. Five conditions previously analyzed via MS analysis were re-investigated with WB. In addition to these conditions, new USMB conditions, with various pressures and times, were analyzed via WB alone. The western blot fold changes ( $FC_{WB}$ ) are shown for (B) HMOX1, (C) BACH-1 and (D) ANXA1, and their corresponding MS fold change ( $FC_{MS}$ ) in (E) to (G), respectively. Plotted are the mean  $\pm$  SD are shown for  $n = 3$  independent experiments. P value threshold represented by \*  $p \leq 0.05$ , \*\*  $p \leq 0.01$ , and \*\*\*  $p \leq 0.001$ .

the user, matches the proteins to one or more cellular components or functions. The analysis (repeat condition) focused on the cellular components with a  $p$ -value  $\leq 0.05$  and an interaction value of  $\geq 5\%$ . The 5% interaction value corresponds to 84 out of 1683 for the statistically identified proteins, and 4 out of 78 for the DEP78 that is mapped to a specific cellular component. Figure 6A shows the analysis of the 1683 statistically identified proteins, which includes the DEP<sub>78</sub>, and the analysis of DEP<sub>78</sub> alone. The cellular components discovered by running DAVID analyses using Table S1 DEPs for USMB conditions, involved components that are known to be affected by USMB. Components such as the extracellular region, and exosomes as well as the PM were affected the most (GO definitions found in Table S3). Compared to statistically identified proteins, DEP<sub>78</sub> revealed that there was nearly no effect on the proteins expressed in and around the nucleus based on the GO classification of "Cellular Component". Components discovered by running DAVID with statistically identified proteins, such as the nucleus, nucleoplasm and nucleolus, fall under outside the inclusion thresholds ( $p \leq 0.05$ ,



and % interaction  $\geq 5\%$ ) when DEP78 were analyzed. To assess the effect of the treatment conditions on the GO cellular components, the DEPs from the list of DEP<sub>78</sub> for each of the USMB conditions (Table S1) were analysed (Fig. 6B). The USMB treatment pressure and elapsed-time affect the GO cellular components (Fig. 6B). As more time elapses post treatment, it appears that there may be changes in expression of proteins with GO annotation of plasma membrane or membrane, whereas the changes in protein expression of proteins with GO annotation of “cytosol” do not appear to change robustly as of 6 h post USMB. In addition, DAVID analyses were run using DEPs from the list of DEP<sub>14</sub> (Table 1) for each USMB condition, and all condition combinations; a detailed

◀ **Fig. 6.** (A) Radar graph of GO terms generated by running DAVID Bioinformatics with DEP<sub>78</sub> and statistically identified proteins, separately. *Statistically identified proteins correspond to Detected Proteins which were discovered to be statistically significant compared to the untreated control.* Values on the chart correspond to the percentage of proteins from a particular DAVID analysis, which are mapped to a particular GO term. GO terms were included if they had a p-value of  $\leq 0.05$  and  $\geq 5\%$  of proteins from their respective lists attributed to them. (B) Radar graph of GO terms generated by running DAVID Bioinformatics with DEPs for each USMB condition separately (DEPs listed in Table S1). Values on the chart correspond to the percentage of proteins from a particular DAVID analysis, which are mapped to a particular GO term. GO terms were selected if they had a p-value of  $\leq 0.05$  and  $\geq 5\%$  of proteins from their respective lists attributed to them. (C) A heatmap with the combined results of DAVID Bioinformatics, run with DEPs for each USMB condition. DEPs of interest (Table 1) from the USMB<sub>450kPa,6 h</sub> (DEP14), USMB<sub>750kPa,6 h</sub> and USMB<sub>750,24 h</sub> conditions were entered into DAVID Bioinformatics separately; a list of GO terms was generated for each group of DEPs. GO results were counted as “hits” if they had a p-value of  $\leq 0.05$  and if the number of proteins in each list attributed to a particular GO term was  $\geq 5\%$ . Results for each condition were plotted on one heatmap; overlapping hits are denoted by unique colours. (AJ – Adherens Junction; APM – Apical Plasma Membrane; BM – Blood Microparticle; ER – Endoplasmic Reticulum; ES – Extracellular Space; FA – Focal Adhesion; GA – Golgi Apparatus; IMBO – Intracellular Membrane-Bounded Organelle; PRC – Perinuclear Region of Cytoplasm; PM – Plasma Membrane; RNAP2TRC – RNA Polymerase II Transcription Regulator Complex).

breakdown is presented in the form of a heatmap in Fig. 6C. The extracellular exosomes appear to be affected at all conditions, whereas the plasma membrane appear to be mostly affected by 24 h following USMB.

## Discussion

### USMB proteome changes

USMB induces a broad spectrum of changes in the AML cell proteome under exposure conditions where a significant sonoporation-bioeffect was observed, such as the presence of microbubbles. This indicates that the main mechanism of USMB-mediated bioeffects at pulsed therapeutic ultrasound exposure conditions is associated with US-mediated cavitation of MBs<sup>18,32,33</sup>. As seen in the flow cytometry assays, USMB significantly enhances uptake of extracellular molecules in AML cells which would otherwise be excluded while having a minimal effect on cell viability; this agrees with other sonoporation studies<sup>10,11,34</sup>. In addition to the presence of microbubbles, modulation of the cell proteome depended on the acoustic pressure. While the sonoporation-bioeffect where cell permeability increased with acoustic pressure to a plateau, the changes observed in the cell proteome varied with the acoustic pressure less predictably. These changes include the specific proteins which are differentially expressed, the number of DEPs and the fold changes in the expression of proteins (DEPs). Furthermore, the time following USMB exposure strongly influences the number of proteins which are differentially expressed and the magnitude of fold change for certain DEPs. This suggests that USMB treatment conditions may be tailored to optimize the expression of a specific DEP of interest in developing cancer therapeutic targets or enhancing existing therapies.

### USMB Bioeffects and DEP<sub>14</sub>

The cellular bioeffects induced by USMB appears to be associated with the differentially expressed proteins; here, we focus on the DEP<sub>14</sub>. The major cellular components associated with USMB-induced DEPs, are generally linked with extracellular and membrane environments and processes based on the analysis of MS data with DAVID bioinformatics; these observations can be potentially induced by USMB<sup>9,10</sup>. These cellular components are associated with membrane disruption, endocytosis and exocytosis (Table S3). This is consistent with USMB induced stress on the cell membrane, which leads to various bioeffects such as membrane disruption, cytoskeleton organization, calcium influx, enhanced endocytosis and oxidative stress<sup>6,8,34</sup>. This may suggest that the proteome changes in the sonoporated cells may be more significant compared to the non-sonoporated cells, and as such, the fold change in the protein expression in sonoporated cells may be significantly higher; this is a focus of future studies.

USMB has been shown to interact with the cell membrane<sup>8,9,16</sup>. Cells alter the expression of cytoskeletal and structural proteins, such as vimentin (VIM)<sup>35</sup> and prelamin-A/C (LMNA)<sup>36–38</sup> in response to stress<sup>39,40</sup>. These proteins exhibit elevated expression following USMB (LMNA increases expression by two-fold).

In addition, ANXA1, S100-A10, S100-A11 and THBS1 are overexpressed following USMB exposure and are related to calcium influx<sup>41–44</sup>. Calcium influx is associated with USMB-mediated disruption of the plasma membrane<sup>8,21</sup>. Calcium is a mediator of various cellular functions including proliferation, motility and mitosis and regulator of various protein families involved in plasma membrane fusion and repair<sup>8,44</sup>. Annexin-A1's high expression across all USMB conditions can be explained as Annexin's are a calcium-binding protein, that can respond to increases in intracellular calcium<sup>43–45</sup>. In addition, calcium alone has not been shown to drive expression of ANXA1<sup>47</sup>, rather it aids in ANXA1's ability to bind to membranes<sup>45</sup>. There is a connection between ANXA1 and apoptosis, as cell death was associated with increased levels of ANXA1 in the cytosol and in the membrane of cells<sup>46</sup>. Similarly, Thrombospondins are calcium-binding glycoproteins that interact with other extracellular matrix components<sup>42</sup>. Its multifunctionality allows THBS1 to assemble multiprotein complexes at the cell surface modulating cell behaviour<sup>47</sup>.

USMB increases cellular ROS after treatment and causes Ca<sup>2+</sup> uptake<sup>6</sup>. This mechanism may be associated with the high fold change observed in HMOX1 in cells treated with USMB. Proteins such as HMOX1, VIM and NQO1 can experience changes in their expression by their involvement in redox reactions and oxidative

stress<sup>40,48,49</sup>. They can be influenced by their involvement in the regulation of ROS<sup>50,51</sup> or their ability to protect the cell from ROS<sup>49</sup>, which are produced during USMB<sup>6</sup>. NQO1 is a coenzyme that is involved with many cellular processes such as proliferation and cell growth<sup>52</sup>. It protects the cell from oxidative stress by inhibiting the production of free radicals<sup>48</sup>. In addition, HMOX1 is upregulated in response to oxidative stress<sup>49,53</sup>. HMOX1 expression is primarily stimulated by heme and oxidative stress<sup>53</sup>. BACH1 is a transcription factor (TF) that acts as a repressor to the HMOX1 gene, HMOX1<sup>54</sup>. It has the capacity to bind to specific promoter sites called stress-responsive elements (StREs), inhibiting the transcription of the HMOX1 gene<sup>54</sup>. Heme driven HMOX1 expression is conferred via binding of heme to BACH1, subsequently causing conformational change in BACH1; this reduces BACH1's affinity to StREs, leading to its nuclear export, and degradation<sup>54</sup>. The elevated level of ROS activates Nrf2 which positively regulates HMOX1 transcription<sup>54,55</sup>. In addition, proteins such as GAS7 and MTSS1, which we observe to have increased expression following USMB, are involved with microfilaments<sup>56</sup> and actin filaments in the membrane<sup>57</sup>. GAS7 proteins can promote actin assembly and filament crosslinking<sup>56</sup>. MTSS1 plays a large part in the upkeep of cell–cell adhesions<sup>58</sup>.

### Therapeutic potential of USMB-mediated DEPs

This study suggests the potential of a novel strategy for utilizing USMB that can be applied selectively (i.e. within a confined tissue) in modulating the cell proteomics, which is dynamically regulated and affects the cell's function. The cell proteome may strategically be modulated by USMB and combined with other therapies such as chemotherapy, immunotherapy and radiotherapy in enhancing therapeutic outcome of cancer<sup>12,14,15</sup>, while simultaneously, enhancing targeted drug delivery to the disease site<sup>8,10,13,28,34</sup>. Therapeutic drug targets for AML have been proposed for multiple DEPs which can be modulated by USMB<sup>59–62</sup>. S100 and Annexin protein families, where USMB increased their expression, are promising therapeutic targets<sup>63–66</sup>. A prognostic study found a positive correlation between ANXA1 expression and favorable outcomes in 60 de novo AML patients<sup>67</sup>, and the increased expression induced by USMB may sensitize cells to apoptosis. In ovarian cancer cells (SKOV3 and A2780), the knockout of S100-A10 resulted in significant reduction of proliferation and increased apoptosis with carboplatin<sup>68</sup>. Future work will investigate selective DEPs as therapeutic targets.

### Conclusions

The application of USMB induced a broad spectrum of changes in the AML cell proteome. The protein expression depended on the ultrasound exposure parameters and varied with time following USMB. A significant modulation in the cell proteome was observed following exposure to ultrasound only in the presence of microbubbles, similar to the sonoporation bioeffect. USMB significantly enhanced the uptake of extracellular molecules in AML cells which otherwise would be excluded with little effect on cell viability. When considering the effects of acoustic pressure, the peak of protein expression varies, with the highest fold change for certain DEPs being achieved at higher acoustic pressures. The number of DEP and their magnitude of expression change, varied less predictably with the acoustic pressure, while the time following USMB exposure strongly influences the number of proteins which are DE. This suggests that USMB treatment conditions may be tailored to optimize the expression of the specific DEP of interest in developing cancer therapeutic targets or enhance existing therapies. Proteins such as HMOX1, ANXA1 and S100A10 and A11 may have potential to be used as drug targets and combined with USMB for enhanced therapeutic effect in cancer.

### Data availability

The datasets used and/or analysed during the current study available from the corresponding author on reasonable request.

Received: 5 March 2025; Accepted: 4 August 2025

Published online: 14 August 2025

### References

- Torres-Martinez, Z. et al. Key genes and drug delivery systems to improve the efficiency of chemotherapy. *Cancer Drug Resist.* **4**(1), 163. <https://doi.org/10.20517/CDR.2020.64> (2021).
- Somero, G. N. The cellular stress response and temperature: Function, regulation, and evolution. *J. Exp. Zool. A Ecol. Integr. Physiol.* **333**(6), 379–397. <https://doi.org/10.1002/JEZ.2344> (2020).
- Harper, C. E. et al. Mechanical stimuli activate gene expression via a cell envelope stress sensing pathway. *Sci. Rep.* **13**(1), 1–12. <https://doi.org/10.1038/s41598-023-40897-w> (2023).
- Poljšak, B. & Milisav, I. Clinical implications of cellular stress responses. *Bosn. J. Basic Med. Sci.* **12**(2), 122. <https://doi.org/10.17305/BJBMS.2012.2510> (2012).
- Jolly, C. & Morimoto, R. I. Stress and the cell nucleus: dynamics of gene expression and structural reorganization. *Gene Expr.* **7**, 261 (1999).
- Przystupski, D. & Ussowicz, M. Landscape of Cellular Bioeffects Triggered by Ultrasound-Induced Sonoporation. *Int. J. Mol. Sci.* **23**(19), 11222. <https://doi.org/10.3390/IJMS231911222> (2022).
- Padilla, F., Brenner, J., Prada, F. & Klibanov, A. L. Theranostics in the vasculature: bioeffects of ultrasound and microbubbles to induce vascular shutdown. *Theranostics* **13**(12), 4079. <https://doi.org/10.7150/THNO.70372> (2023).
- Lentacker, I., De Cock, I., Deckers, R., De Smedt, S. C. & Moonen, C. T. W. Understanding ultrasound induced sonoporation: Definitions and underlying mechanisms. *Adv. Drug. Deliv. Rev.* **72**, 49–64. <https://doi.org/10.1016/j.addr.2013.11.008> (2014).
- Hussein, F., Antonescu, C. & Karshafian, R. Ultrasound and microbubble induced release from intracellular compartments. *BMC Biotechnol.* **17**(45), 1–12. <https://doi.org/10.1186/s12896-017-0364-3> (2017).
- Karshafian, R., Samac, S., Bevan, P. D. & Burns, P. N. Microbubble mediated sonoporation of cells in suspension : Clonogenic viability and influence of molecular size on uptake. *Ultrasonics* **50**(7), 691–697. <https://doi.org/10.1016/j.ultras.2010.01.009> (2010).
- Fekri, F., Delos Santos, R. C., Karshafian, R. & Antonescu, C. N. Ultrasound microbubble treatment enhances clathrin-mediated endocytosis and fluid-phase uptake through distinct mechanisms. *PLoS ONE* **11**(6), 1–22. <https://doi.org/10.1371/journal.pone.0156754> (2016).



12. Sharma, D., Leong, K. X. & Czarnota, G. J. Application of ultrasound combined with microbubbles for cancer therapy. *Int. J. Mol. Sci.* **23**(8), 4393. <https://doi.org/10.3390/IJMS23084393> (2022).
13. Hernot, S. & Klivanov, A. L. Microbubbles in ultrasound-triggered drug and gene delivery. *Adv. Drug Deliv. Rev.* **60**(10), 1153–1166. <https://doi.org/10.1016/j.addr.2008.03.005> (2008).
14. Chowdhury, S. M., Abou-Elkacem, L., Lee, T., Dahl, J. & Lutz, A. M. Ultrasound and microbubble mediated therapeutic delivery: Underlying mechanisms and future outlook. *J. Control. Release* **326**, 75–90. <https://doi.org/10.1016/J.JCONREL.2020.06.008> (2020).
15. Sharma, D., McNabb, E., Law, N., Cumal, A. & Czarnota, G. J. Ultrasound-stimulated microbubbles enhancement of fractionated radiation for tumor treatment. *BMC Cancer* **23**(1), 1–10. <https://doi.org/10.1186/S12885-023-10981-5/FIGURES/6> (2023).
16. Guzmán, H. R., Nguyen, D. X., Khan, S. & Prausnitz, M. R. “Ultrasound-mediated disruption of cell membranes I. quantification of molecular uptake and cell viability. *J. Acoust. Soc. Am.* **110**(1), 588. <https://doi.org/10.1121/1.1376131> (2001).
17. Lo, L., Uchenunu, O., Botelho, R. J., Antonescu, C. N. & Karshafian, R. AMPK is required for recovery from metabolic stress induced by ultrasound microbubble treatment. *iScience*. **26**, 2. <https://doi.org/10.1016/J.ISCI.2022.105883> (2022).
18. Fan, Z., Kumon, R. E. & Deng, C. X. Mechanisms of microbubble-facilitated sonoporation for drug and gene delivery. *Ther. Deliv.* **5**(4), 467–486. <https://doi.org/10.4155/TDE.14.10> (2014).
19. Bouakaz, A., Zeghimi, A. & Doinikov, A. A. Sonoporation: Concept and Mechanisms. *Adv. Exp. Med. Biol.* **880**, 175–189. [https://doi.org/10.1007/978-3-319-22536-4\\_10](https://doi.org/10.1007/978-3-319-22536-4_10) (2016).
20. Höhfeld, J. et al. Maintaining proteostasis under mechanical stress. *EMBO Rep.* **22**(8), 1–22. <https://doi.org/10.15252/embr.202152507> (2021).
21. Juffermans, L. J. M. et al. Ultrasound and microbubble-induced intra- and intercellular bioeffects in primary endothelial cells. *Ultrasound Med. Biol.* **35**(11), 1917–1927. <https://doi.org/10.1016/j.ultrasmedbio.2009.06.1091> (2009).
22. De Cock, I. et al. Ultrasound and microbubble mediated drug delivery: acoustic pressure as determinant for uptake via membrane pores or endocytosis. *J. Control Release* **197**, 20–28. <https://doi.org/10.1016/J.JCONREL.2014.10.031> (2015).
23. Tardoski, S. et al. Low-intensity ultrasound promotes clathrin-dependent endocytosis for drug penetration into tumor cells. *Ultrasound Med. Biol.* **41**(10), 2740–2754. <https://doi.org/10.1016/J.ULTRASMEDBIO.2015.06.006> (2015).
24. Zhong, W., Sit, W. H., Wan, J. M. F. & Yu, A. C. H. Sonoporation induces apoptosis and cell cycle arrest in human promyelocytic leukemia cells. *Ultrasound Med. Biol.* **37**(12), 2149–2159. <https://doi.org/10.1016/J.ULTRASMEDBIO.2011.09.012> (2011).
25. Haugse, R. et al. Low-intensity sonoporation-induced intracellular signalling of pancreatic cancer cells, fibroblasts and endothelial cells. *Pharmaceutics* **12**(11), 1–17. <https://doi.org/10.3390/PHARMACEUTICS12111058> (2020).
26. Chen, Y., Ju, L., Rushdi, M., Ge, C. & Zhu, C. Receptor-mediated cell mechanosensing. *Mol. Biol. Cell* **28**(23), 3134–3155. <https://doi.org/10.1091/mbc.E17-04-0228> (2017).
27. Li, G. & Qian, H. Sensitivity and Specificity Amplification in Signal Transduction. *Cell Biochem. Biophys.* **39**, 45–59 (2003).
28. Karshafian, R., Bevan, P. D., Williams, R., Samac, S. & Burns, P. N. Sonoporation by ultrasound-activated microbubble contrast agents: effect of acoustic exposure parameters on cell membrane permeability and cell viability. *Ultrasound Med. Biol.* **35**(5), 847–860. <https://doi.org/10.1016/J.ULTRASMEDBIO.2008.10.013> (2009).
29. Schindelin, J. et al. Fiji: an open-source platform for biological-image analysis. *Nat. Methods* **9**(7), 676–682. <https://doi.org/10.1038/nmeth.2019> (2012).
30. Huang, D. W., Sherman, B. T. & Lempicki, R. A. Systematic and integrative analysis of large gene lists using DAVID bioinformatics resources. *Nat. Protoc.* **4**(1), 44–57. <https://doi.org/10.1038/NPROT.2008.211> (2009).
31. Sherman, B. T. et al. DAVID: a web server for functional enrichment analysis and functional annotation of gene lists (2021 update). *Nucleic Acids Res.* **50**(W1), W216–W221. <https://doi.org/10.1093/NAR/GKAC194> (2022).
32. Qiu, Y., Zhang, C., Tu, J. & Zhang, D. Microbubble-induced sonoporation involved in ultrasound-mediated DNA transfection in vitro at low acoustic pressures. *J. Biomech.* **45**(8), 1339–1345. <https://doi.org/10.1016/J.JBIOMECH.2012.03.011> (2012).
33. Yang, Y., Li, Q., Guo, X., Tu, J. & Zhang, D. Mechanisms underlying sonoporation: Interaction between microbubbles and cells. *Ultrason Sonochem.* **67**, 105096. <https://doi.org/10.1016/J.ULTSONCH.2020.105096> (2020).
34. Peruzzi, G., Sinibaldi, G., Silvani, G., Ruocco, G. & Casciola, C. M. Perspectives on cavitation enhanced endothelial layer permeability. *Colloids Surf B Biointerfaces* <https://doi.org/10.1016/j.colsurf.2018.02.027> (2018).
35. Hubner, S. et al. Targeting Vimentin (VIM) in Acute Myelogenous Leukemia (AML). *Blood* **140**(Supplement 1), 6260–6261. <https://doi.org/10.1182/BLOOD-2022-163664> (2022).
36. Gruenbaum, Y. & Foisner, R. Lamins: nuclear intermediate filament proteins with fundamental functions in nuclear mechanics and genome regulation. *Annu. Rev. Biochem.* **84**, 131–164. <https://doi.org/10.1146/ANNUREV-BIOCHEM-060614-034115> (2015).
37. Fletcher, D. A. & Mullins, R. D. Cell mechanics and the cytoskeleton. *Nature* **463**(7280), 485. <https://doi.org/10.1038/NATURE08908> (2010).
38. Jones, J. C. R. et al. Intermediate filaments and the plasma membrane. *Cold Spring Harb. Perspect. Biol.* **9**, 1. <https://doi.org/10.1101/CSHPERSPECT.A025866> (2017).
39. Houben, F., Ramaekers, F. C. S., Snoeckx, L. H. E. H. & Broers, J. L. V. Role of nuclear lamina-cytoskeleton interactions in the maintenance of cellular strength. *Biochim. Biophys. Acta. Mol. Cell Res.* **1773**(5), 675–686. <https://doi.org/10.1016/j.bbamcr.2006.09.018> (2007).
40. Riegger, J. & Brenner, R. E. Increase of cell surface vimentin is associated with vimentin network disruption and subsequent stress-induced premature senescence in human chondrocytes. *Elife* <https://doi.org/10.7554/ELIFE.91453> (2023).
41. Jaiswal, J. K. & Nylandsted, J. “S100 and annexin proteins identify cell membrane damage as the Achilles heel of metastatic cancer cells. *Cell Cycle* **14**(4), 502–509 (2015).
42. J. C. Adams, J. Lawler, R. O. Hynes, and K. M. Yamada, “The Thrombospondins,” *Additional Perspectives on Extracellular Matrix Biology*, <https://doi.org/10.1101/cshperspect.a009712>.
43. Cooper, S. T. & Mcneil, P. L. Membrane repair: mechanisms and pathophysiology. *Physiol. Rev.* **95**, 1205–1240. <https://doi.org/10.1152/physrev.00037.2014.-Eukaryotic> (2015).
44. Blazek, A. D., Paleo, B. J. & Weisleder, N. Plasma membrane repair: a central process for maintaining cellular homeostasis. *Physiology* **30**(6), 438. <https://doi.org/10.1152/PHYSIOL.00019.2015> (2015).
45. Gerke, V. & Moss, S. E. Annexins: from structure to function. *Physiol. Rev.* **82**(2), 331–371. <https://doi.org/10.1152/PHYSREV.00030.2001/ASSET/IMAGES/LARGE/9J0220191106.JPEG> (2002).
46. Hatah, E., Yin Hui, P. G. & Kumolosasi, E. Annexin A1 and leukemia: A systematic review. *Tropical J. Pharma. Res.* **18**(12), 2653–2668. <https://doi.org/10.4314/tjpr.v18i12.26> (2019).
47. Kvensakul, M., Adams, J. C. & Hohenester, E. Structure of a thrombospondin C-terminal fragment reveals a novel calcium core in the type 3 repeats. *EMBO J.* **23**(6), 1223–1233. <https://doi.org/10.1038/sj.emboj.7600166> (2004).
48. Preethi, S., Arthiga, K., Patil, A. B., Spandana, A. & Jain, V. 2022 “Review on NAD(P)H dehydrogenase quinone 1 (NQO1) pathway. *Mol. Biol. Rep.* **49**(9), 8907–8924. <https://doi.org/10.1007/S11033-022-07369-2> (2022).
49. Ryter, S. W. & Choi, A. M. K. Heme oxygenase-1: redox regulation of a stress protein in lung and cell culture models. *Antioxid. Redox Signal* **7**(1–2), 80–91. <https://doi.org/10.1089/ars.2005.7.80> (2005).
50. Huynh, T. N. et al. Vimentin regulates mitochondrial ROS production and inflammatory responses of neutrophils. *bioRxiv* <https://doi.org/10.1101/2024.04.11.589146> (2024).



51. Nishida-Tamehiro, K., Kimura, A., Tsubata, T., Takahashi, S. & Suzuki, H. Antioxidative enzyme NAD(P)H quinone oxidoreductase 1 (NQO1) modulates the differentiation of Th17 cells by regulating ROS levels. *PLoS ONE* **17**(7), e0272090. <https://doi.org/10.1371/JOURNAL.PONE.0272090> (2022).
52. Corpas, F. J. & Barroso, J. B. NADPH-generating dehydrogenases: Their role in the mechanism of protection against nitro-oxidative stress induced by adverse environmental conditions. *Front. Environ. Sci.* **2**, 1–5. <https://doi.org/10.3389/fenvs.2014.00055> (2014).
53. Choi, A. M. K. & Alam, J. “Heme oxygenase-1: function, regulation, and implication of a novel stress-inducible protein in oxidant-induced lung injury. *Am. J. Respiratory Cell Mol. Biol.* <https://doi.org/10.1165/ajrcmb.15.1.8679227> (2012).
54. Gozzelino, R., Jeney, V. & Soares, M. P. “Mechanisms of cell protection by heme oxygenase-1”. *Annu. Rev. Pharmacol. Toxicol.* **50**, 323–354. <https://doi.org/10.1146/annurev.pharmtox.010909.105600> (2010).
55. Sadeghi, M. et al. The prognostic and therapeutic potential of HO-1 in leukemia and MDS. *Cell Commun. Signaling* **21**(1), 1–21. <https://doi.org/10.1186/s12964-023-01074-8> (2023).
56. She, B. R., Liou, G. G. & Lin-Chao, S. Association of the growth-arrest-specific protein Gas7 with F-actin induces reorganization of microfilaments and promotes membrane outgrowth. *Exp. Cell Res.* **273**(1), 34–44. <https://doi.org/10.1006/excr.2001.5435> (2002).
57. Grandits, A. M. et al. Downregulation of MTSS1 in acute myeloid leukemia is associated with a poor prognosis, chemotherapy resistance, and disease aggressiveness. *Leukemia* **35**(10), 2827. <https://doi.org/10.1038/S41375-021-01224-2> (2021).
58. Vadakekolathu, J. et al. MTSS1 and SCAMP1 cooperate to prevent invasion in breast cancer. *Cell Death Dis.* **9**, 3. <https://doi.org/10.1038/S41419-018-0364-9> (2018).
59. D’Acunto, C. W. et al. Histone deacetylase inhibitor FR235222 sensitizes human prostate adenocarcinoma cells to apoptosis through up-regulation of Annexin A1. *Cancer Lett.* **295**(1), 85–91. <https://doi.org/10.1016/J.CANLET.2010.02.016> (2010).
60. Ryter, S. W., Alam, J. & Choi, A. M. K. Heme Oxygenase-1/Carbon Monoxide: from basic science to therapeutic applications. *Physiol. Rev.* <https://doi.org/10.1152/physrev.00011.2005.-The> (2006).
61. Sharp, F. R., Zhan, X. & Liu, D. Z. Heat shock proteins in brain: role of Hsp70, Hsp 27 and HO-1 (Hsp32) and their therapeutic potential. *Transl. Stroke Res* **4**(6), 685–692. <https://doi.org/10.1007/S12975-013-0271-4> (2013).
62. Ma, K., Chen, S., Chen, X., Yang, C. & Yang, J. S100A10 is a new prognostic biomarker related to the malignant molecular features and immunosuppression process of adult gliomas. *World Neurosurg* **165**, e650–e663. <https://doi.org/10.1016/J.WNEU.2022.06.124> (2022).
63. Podkalicka, P., Mucha, O., Józkowicz, A., Dulak, J. & Łoboda, A. Heme oxygenase inhibition in cancers: possible tools and targets. *Współczesna Onkologia* **2**(1A), 23–32. <https://doi.org/10.5114/wo.2018.73879> (2017).
64. Hua, X. et al. Roles of S100 family members in drug resistance in tumors: status and prospects. *Biomed. Pharmacother.* <https://doi.org/10.1016/J.BIOPHA.2020.110156> (2020).
65. Wang, X. et al. Targeting annexin A1 as a druggable player to enhance the anti-tumor role of Honokiol in colon cancer through autophagic pathway. *Pharm. Article* **16**, 1–14 (2023).
66. López-Pedrerá, C. et al. Proteomic analysis of acute myeloid leukemia: Identification of potential early biomarkers and therapeutic targets. *Proteomics* **6**(S1), S293–S299. <https://doi.org/10.1002/PMIC.200500384> (2006).
67. Gaber, M., Kasem, A., Azzazi, M., Tarif, M. & Yusuf, E. Prognostic impact of Annexin A1 expression in acute myeloid leukemia. *Egyptian J. Haematol.* **45**(2), 57. [https://doi.org/10.4103/EJH.EJH\\_45\\_19](https://doi.org/10.4103/EJH.EJH_45_19) (2020).
68. Wang, L. et al. S100A10 silencing suppresses proliferation, migration and invasion of ovarian cancer cells and enhances sensitivity to carboplatin. *J. Ovarian Res.* **12**(1), 1–11. <https://doi.org/10.1186/s13048-019-0592-3> (2019).

## Author contributions

JS: Study design, study implementation, data analysis, data visualization, Writing—original draft, editing and review. DA: Data analysis and visualization (DAVID bioinformatics), statistical analysis, Writing—original draft (part of results and discussion), editing and review. ES: Western blot study design and implementation, data analysis and visualization, Writing—editing and review. CF: Study implementation (ultrasound), data analysis, Writing—review. EC: Western blot study implementation, data analysis, Writing—review. RB: Conceptualization, study design, analysis, writing—editing and review. CA: Conceptualization, study design, analysis, writing—editing and review. RK: Supervision, conceptualization, study design and implementation, data analysis, statistical analysis, Writing—editing and review.

## Funding

Natural Sciences and Engineering Research Council (NSERC) Discovery grants program, RGPIN-201505941

## Declarations

## Competing interests

The authors declare no competing interests.

## Additional information

**Supplementary Information** The online version contains supplementary material available at <https://doi.org/10.1038/s41598-025-14727-0>.

**Correspondence** and requests for materials should be addressed to R.K.

**Reprints and permissions information** is available at [www.nature.com/reprints](http://www.nature.com/reprints).

**Publisher’s note** Springer Nature remains neutral with regard to jurisdictional claims in published maps and institutional affiliations.

**Open Access** This article is licensed under a Creative Commons Attribution-NonCommercial-NoDerivatives 4.0 International License, which permits any non-commercial use, sharing, distribution and reproduction in any medium or format, as long as you give appropriate credit to the original author(s) and the source, provide a link to the Creative Commons licence, and indicate if you modified the licensed material. You do not have permission under this licence to share adapted material derived from this article or parts of it. The images or other third party material in this article are included in the article's Creative Commons licence, unless indicated otherwise in a credit line to the material. If material is not included in the article's Creative Commons licence and your intended use is not permitted by statutory regulation or exceeds the permitted use, you will need to obtain permission directly from the copyright holder. To view a copy of this licence, visit <http://creativecommons.org/licenses/by-nc-nd/4.0/>.

© The Author(s) 2025